

RF - SUPERCONDUCTIVITY AT CERN

C. Benvenuti, P. Bernard, D. Bloess, G. Cavallari, E. Chiaveri,
N. Circelli, W. Erdt, E. Haebel, H. Lengeler^(*), P. Marchand, R. Stierlin,
J. Tückmantel and W. Weingarten
CERN, Geneva, Switzerland

and

H. Piel
University of Wuppertal, West Germany

1. INTRODUCTION

In 1979 a feasibility study for the application of superconducting accelerating cavities to LEP was started at CERN [1-3]. From the beginning a special emphasis was put on simple fabrication methods and surface treatments. Cavities are fabricated by spinning from 2 or 3 mm Nb sheets and are assembled by electron beam welding. A chemical polishing (CP) followed by rinsing with clean dustfree water allowed to reach quality factors and accelerating fields considered satisfactory for LEP.

A quasi-spherical shape was chosen and its lower liability to multipactor was confirmed not only in many tests with single cell and multicell cavities [1] but also during operation of a 500 MHz, 5-cell cavity in the PETRA storage ring [4]. This shape has also advantages for applying chemical treatments, rinsings, ion bombardment and sputtering and is well suited for the application of temperature mappings. In addition the mechanical stability of this shape facilitates tuning and frequency regulations and allows to use a small wall thickness.

(*) Presented by H. Lengeler

A strong effort was made to improve the diagnostic methods. Temperature mapping in subcooled helium was developed and proved itself a very valuable method for investigating details of cavity behaviour [1]. We use this method as a standard tool for localising point-like [5] and extended regions of increased r.f. losses and for studying their dependence on field level and temperature. It has allowed to increase our knowledge of electron sources and of resonant and non-resonant electron loading [1,6]. It is possible to follow by temperature mapping the evolution of r.f. losses and electron loading. By now it has been developed to a quantitative method [7] whose precision and reproducibility allows independent determinations of quality factors and field flatness. Its sensitivity has been pushed to ~ 1 mK (corresponding for point-like defects to r.f. losses of ~ 30 μ W) and permits to do temperature maps at field levels well below 1 MV/m (30 G).

The possibility for localising defects and the study of their origins and behaviour allowed to improve welding methods [8] and surface treatments [9] and showed the importance of rinsing with clean, dust-free water and mounting under dust-free conditions. It also opened the way for guided repair of defects before the first cooldown. These improvements and the application of He-ion sputtering allowed to raise accelerating fields in 500 MHz single-cell and multicell cavities gradually to about 5 MV/m (fig. 1), the fields being limited in most cases by a defect at the welds. A new step in upgrading fields was reached when Nb material with improved thermal conductivity became available which stabilizes defects thermally in a more efficient way [10-12]. Fields up to 13 MV/m were reached in 500 MHz single-cell cavities fabricated with the new Nb material.

Besides these Nb cavity developments the sputtering of thin Nb layers on Cu cavities was pursued [13,14]. The absence of any quenches up to the highest field levels reached (8.6 MV/m), and the possibility of other cooling schemes i.c. cooling by tubes or by partial immersion in a LHe bath makes this development extremely interesting.

Since the start of the programme, work with 3 GHz cavities has always been continued as a back-up of cavity developments. In all, 21 single-cell

cavities have been tested and 9 of them have been cut to pieces to obtain additional informations on surface defects [5], lossy regions and welds. Also sputtering of Nb layers onto Nb was investigated. A large part of the tests have been devoted to improve the surface treatments and rinsing facilities.

The test of a 500 MHz, 5-cell cavity at PETRA [4] asked for the development of main couplers [14], Higher Order Mode (HOM) couplers [14-15] and a tuning system [16]. The cavity was equipped with one HOM coupler on each cell and with a mechanical tuning system acting on the two end cells (fig. 2(a)). The analysis of the cavity behaviour and of test results led to a new cavity design [17,18] where the main coupler and the HOM couplers are located at the beam tubes (fig. 2(b) and table 1). This will allow a more economic fabrication of cavities and will reduce the danger of multipactor known to occur at coupling ports located in equatorial regions [16] and will simplify temperature mapping. A much simplified hydraulic tuner for this new cavity design acting on the total cavity length has already been tested. The advent of new and improved computer programmes [19,20] for cavity calculations gave us for the first time the possibility to compute not only all monopole modes but also multipole in the multi-cell cavity. In this way it became possible to device a new multi-mode compensation scheme for end cells which is crucial for the coupling at the beam tubes [17,18].

Besides the 500 MHz programme the development of 350 MHz cavities has been pushed forward [21,3]. LEP will be equipped in a first stage with 128 five-cell Cu cavities and an r.f. power of 16 MW will be installed [22]. In conjunction with s.c. cavities this r.f. power would be sufficient for on upgrading of LEP to ~ 80 GeV/c. It is therefore of obvious interest to strive for the same frequency as for the Cu cavities. In addition, impedances and in particular transverse impedances which are known to limit the stored current in LEP [23] can be reduced by the use of lower frequencies. In 350 MHz single-cell cavities fabricated with "low" heat conductivity Nb material, fields of 5.4 MV/m with an excellent quality factor $Q_0 > 3 \times 10^9$ at 4.2 K have been reached repeatedly. The limit at 5.4 MV/m shows characteristics of a resonant electron phenomenon [24] and it remains to be seen if the use of Nb-material with higher

thermal conductivity will help to overcome this limit and to reach field levels similar to the ones achieved in our 500 MHz cavities.

The continuous increase of fields in 500 MHz and 350 MHz cavities has only been possible by the developments of new installations for chemical treatments (fig. 3), dust-free rinsing with ultrapure water and assembling under dust-free laminar flow conditions [9]. A great effort has been made also together with the CERN workshops for improving the electron and TIG welding facilities [8]. The measurements of s.c. cavities were improved and automatized. Computer controlled measuring set-ups were developed which allow to measure and plot Q values, electron currents, coupling factors etc. as a function of the accelerating fields. In this way it became possible to investigate the cavity behaviour in greater detail and with increased accuracy and reproducibility.

Cryostats and their auxiliary equipment will present a major part in the investment costs of s.c. cavities. At CERN, simple and economic cryostat layouts are studied and first test cryostats involving new constructive solutions are under progress [25].

2. LATEST EXPERIMENTAL RESULTS

2.1 New results with a 500 MHz, 5-cell cavity

In March-April 1983 a 500 MHz, 5-cell cavity had been installed and operated in the PETRA storage ring at DESY [4]. The operation of the s.c. cavity at various operating conditions with standard PETRA control and regulation elements presented no major technical difficulties. The HOM behaviour confirmed predictions and no unexpected effects in beam stability have been observed up to the maximum available current of 8 mA. Contrary to observations during tests at CERN [16] (where the cavity was equipped with a low power coupler of $Q_{\text{ext}} = 10^9$) no multipactor effects were observed during operation at PETRA. This may be partly explained by the strong coupling of the high power coupler ($Q_{\text{ext}} = 10^6$) needed for operation with the beam.

Due to a very tight time schedule and to the non-availability of an adequate chemical treatment facility the cavity could not be submitted

after welding to an integral chemical polishing and fields were limited to 2.8 MV/m with $Q_0 = 10^9$ at 4.2 K. As the cavity was not equipped with a T-mapping system but only with 40 fixed resistors it was not possible to locate the field limiting defects precisely. After its return to CERN the cavity was inspected, defect regions were reground and an integral CP of 50 μm in a new surface treatment installation (fig. 2) was applied. Afterwards the cavity was rinsed as usually with high purity, dust-free water ($\rho = 18.2 \text{ MOhm} \times \text{cm}$), dried in horizontal position inside a dust-free hut and connected under laminar flow conditions to its vacuum system. The measurement was performed in a vertical cryostat (without the main couplers and the HOM couplers, fig. 4).

In contrast to the results of the two first tests before installation in PETRA, the maximum field of 5 MV/m could be reached within 1 h. Some low multipacting levels and some quenches due to electron activity were overcome rapidly. We attribute the small electron activity to the improved chemical polishing and to the final rinsing with very clean water. This result is the more remarkable as the cavity was measured in vertical position where it is more prone to electron activity than in the horizontal position. The field was limited at 4.2 K by a defect located at the main coupler port with $Q_0 = 0.74 \times 10^9$. This test has confirmed that the field limitations previously observed were only due to an inadequate quality of the (local) CP applied and that again no field limitations specific for multi-cell cavities were found.

During the test at PETRA the Q_0 degraded from an initial 10^9 to 5×10^8 and could not be restored by a warm up to 80°C for 12 h. In addition, a new quench developed at the bottom of cell 2. At the warm up a considerable gas desorption from the cavity was observed, corresponding to at least 200 monolayers of gas covering the cold walls and originating from the warmer parts of the cavity (like couplers and beam tubes) and from the adjacent beam components, in particular from the Cu-cavities. An inspection of the cavity revealed large area stains, some of them located at the quench regions. The analysis by SEM and SIMS revealed as a main constituent non-water soluble phosphates. It was possible to reproduce similar stains [9] in a 3 GHz and in a 500 MHz single-cell cavity and it was shown that neither the Q_0 values nor the fields were deteriorated

with respect to normally treated cavities ($Q_0 = 1.2 \times 10^9$ at 4.2 K and $E_{acc} = 8$ MV/m). Therefore, we think that we can rule out phosphates as a cause and that the most probable source of defects and Q_0 degradation is the cryopumping of (non-dust-free) gases.

In order to clarify this point and to define precisely vacuum and dust conditions necessary for s.c. cavities in LEP, a test programme for gas and dust exposures has been started. In a first test a 500 MHz cavity was exposed at LHe temperatures to increasing amounts of dust-free laboratory air. Some results are given in fig. 5. Exposures corresponding to 300 monolayers of air increase already considerably electron loading but affect only slightly Q_0 . These deteriorations could not be restored by a warm up to 80°C. Much larger exposures ($\sim 10^4$ monolayers) are necessary for decreasing Q_0 values by a factor 2. It is intended to continue these tests and to check whether r.f. processing, He-ion sputtering and/or a warm up to temperatures well above 100°C can cure these degradations.

2.2 500 MHz cavities fabricated from Nb sheets with increased thermal conductivity

The insight in the role of heat conductivity λ for defect stabilisation [10-12] has already triggered some developments in the fabrication of Nb sheet material where λ is increased from a typical 5-10 W/K x m to 28 W/K x m at 4.2 K^(*) (residual resistance ratio rrr = 110). It was checked with a measuring set-up for λ at CERN [26] that these values are not decreased substantially at the electron beam welds and for cold worked material.

Two single-cell 500 MHz cavities have been fabricated and surface treated according to our standard procedures. Five tests were performed with cavity 1 and one test with cavity 2. In table 2 a few results are presented. The analysis of these measurements is still going on [24] and the following preliminary summary can be given.

In both cavities it was possible to reach after a short r.f. processing fields in excess of 8 MV/m exceeding significantly fields

(*) Manufactured by W.C. Heraeus, G.m.b.H, Hanau, W. Germany.

achieved up to now. In the region of 8-9 MV/m strong electron loading sets in which seems to involve electron multiplication around the equator region and whose nature is not yet fully understood. An He-ion sputtering did not allow to raise the field above these levels. Many quenches involving electron activity at low and high fields are also observed.

Following on idea put forward in ref. [27], the first cavity was anodized (at 100 V) and rinsed by ultrapure water in the usual way. During field increase some quenches due to electrons were observed. Between 8 and 9 MV/m similar phenomena as before were observed, but could be overcome rapidly by r.f. processing up to 10 MV/m. A subsequent He processing of 2 h allowed to reach 13 MV/m with $Q_0 = 7 \times 10^8$ at 4.2 K. Later on the field stabilized at ~ 12.7 MV/m. The field was limited by a quench (whose precursor can be seen at 12.6 MV/m but not at 8.6 MV/m) and which is probably due to electrons [24]. The Q_0 dependence on field is shown in fig. 6 and a temperature map in fig. 7.

For the next experiment the anodization layer was removed by concentrated HF and a new rinsing was applied. Results confirm essentially the ones obtained with anodization. The Q_0 values at 4.2 K and low field range for cavity 1 between $1.2 - 1.5 \times 10^9$ and are known to be limited by the Cu covers of the (shortened) beam tubes [28]. For cavity 2 these losses can be neglected and one got $Q_0 = 1.6 \times 10^9$ at 4.2 K and $Q_0 = 5.7 \times 10^9$ at 2.6 K. In the first three experiments with cavity 1 only three defects with increased r.f. losses were visible before He-ion sputtering but 12 more were produced during He-ion sputtering, of which two were situated at a (visible) electron trajectory and three situated at the weldings. Some of them disappeared at later stages of the experiment. The power dissipation of these spots was determined from the temperature maps. Within the statistics available, the dissipation range of defects is not different from the ones observed earlier with the "low λ " material and the improvement in fields can therefore be allocated to the increased λ . Taking as a reference the highest field level reached at 4.2 K in a 500 MHz single cell cavity ($E_{\max} = 7.6$ MV/m and $\lambda_1 = 10.5$ W/K/m [28]) and by assuming a $\sqrt{\lambda}$ dependence for a defect limited field [10], one gets for the new material ($\lambda_2 = 28$ W/K \times m) $E_{\max} = 12.4$ MV/m in good agreement with the experimental results.

In fig. 8 we show the computed behaviour of a typical defect for Nb material with different λ . For comparison we also show the behaviour for the same defect in a Nb-Cu cavity, where $\lambda = 485 \text{ W/m} \times \text{K}$ is more than an order of magnitude higher than for the Nb material. It can be shown, and it has been demonstrated experimentally, that the λ of the present niobium material is not sufficient to cool by heat conduction a half immersed cavity for fields of $\sim 5 \text{ MV/m}$. In order to apply this cooling method or cooling by tubes fixed to the cavity wall, with only 1 or 2 tubes per cell, the much higher λ of a Nb-Cu cavity will be needed.

2.3 350 MHz test cavities for LEP

Up to now two single-cell 350 MHz cavities (fig. 9) have been constructed and tested [21,3]. They are fabricated from 3 mm Nb sheet material (with $\lambda = 10.5 \text{ W/m} \times \text{K}$ at 4.2 K) and the standard surface treatments were applied. The first cavity was scaled from the 500 MHz design for PETRA. For the second cavity the improved geometry for LEP was chosen and the cavity was EB welded with an internal gun^(*). Both cavities are equipped with shortened beam tubes so as to allow measurement in horizontal position inside a vertical cryostat.

At fig. 10 typical field dependences of Q_0 values are shown and in tables 1 and 2 a few parameters and results are given. Cavity No. 1 was limited at $E_{\text{acc}} = 5.4 \text{ MV/m}$ (4.2 K) by an electron induced quench involving some electron resonance phenomena at the equator region [24]. At 2.3 K this quench was overcome and a field of 6.4 MV/m was reached which was limited by a defect at the welding but seemed to involve also some electron loading at the equator.

Cavity No. 2 showed like cavity No. 1 many low level electron activities which could be overcome by a few hours of r.f. processing. He-ion sputtering allowed to reach 5.4 MV/m where an electron induced quench located at the bottom part of the equator limited the field. For the second test the cavity was anodized (100 V). Contrary to the behaviour of 500 MHz cavities the anodization increased the electron activity. At 5.6 MV/m a strong threshold involving again an

(*) Lent kindly to us by Sciaky, Paris.

electron resonance phenomena located at the bottom part of the equator limited the field. This limit could not be overcome neither by r.f. processing and He-ion sputtering nor at lower bath temperature. The analysis of these field limitations is going on.

Temperature mapping (fig. 11) reveals that the r.f. losses are dominated by the losses due to the external magnetic field of 130 mG [21]. By taking into account these losses one determines a mean r.f. resistance at 4.2 K, $R_s < 54 \text{ n Ohm}$ ($Q_o > 5 \times 10^9$). Because of the shortened beam tubes the r.f. losses at the copper beam tube covers and at their r.f. joints (Pb) cannot be avoided. It is therefore estimated that the surface resistance approaches the theoretical limit $R_{BCS} = 37 \text{ n Ohm}$ ($Q_o = 7.3 \times 10^9$) at 4.2 K. These Q_o values are substantially higher than the ones obtained with 500 MHz cavities (c.f. above) and can be considered another argument in favour of 350 MHz cavities because they overcompensate the decrease of R/Q with frequency (R: shunt impedance) and allow reduced losses per unit length of cavities.

3. OUTLOOK

Our programme for the immediate future will concentrate on the field limitations around 5.4 MV/m, observed in 350 MHz cavities. A 4-cell Cu cavity of 350 MHz has been fabricated and r.f. measurements for checking the behaviour of the improved geometry for LEP have started. A 350 MHz 4-cell cavity with high thermal conductivity will be fabricated and tested as soon as possible. The results of these experiments may influence the final decision about the operating frequency for s.c. cavities in LEP. It is hoped that in 1985 contacts with industry for the fabrication of cavities, cryostats and cryogenics can be started on a larger scale.

Acknowledgements

We would like to thank all technicians of our groups for their help. We also would like to thank the Cryogenic Group, BEBC and the Workshop of EF Division, the Vacuum Group of LEP division as well as the workshops for sheet metal work, chemistry, EB welding, brazing and surface inspection.

REFERENCES

- [1] Ph. Bernard et al., Nucl. Instr. & Meth. 190 (1981) 257.
- [2] Ph. Bernard et al., Nucl. Instr. & Meth. 206 (1983) 47.
- [3] C. Benvenuti et al., CERN/EF/RF 84-3 (1984).
- [4] Ph. Bernard et al., Proceedings 12th Int. Conf. High Energy Acc., Fermilab 1983, 244 (1983).
- [5] H. Padamsee, J. Tückmantel and W. Weingarten, CERN/EF 82-17 and IEEE MAG 19, 3 (1983) 1308.
- [6] J. Tückmantel and W. Weingarten, CERN/EF 82-6 (1982).
- [7] R. Romijn, W. Weingarten and H. Piel, CERN/EF 83-1 and IEEE MAG 19, 3 (1983) 1318.
- [8] E. Chiaveri and H. Lengeler, this Workshop.
- [9] D. Bloess, this Workshop.
- [10] H. Padamsee, CERN/EF 82-5 and IEEE MAG 19, 3 (1983) 1322.
- [11] J. Tückmantel CERN/EF/RF 84-7 (1984).
- [12] J. Tückmantel, to be published.
- [13] C. Benvenuti, N. Circelli and M. Hauer, to be published in Appl. Phys. Letter and CERN/LEP Note 490, March 1984.
- [14] C. Benvenuti, this Workshop.
- [15] E. Haebel, CERN/EF/RF 83-4.
- [16] Ph. Bernard et al., IEEE NS-30 (1983) 3342.
- [17] E. Haebel, P. Marchand and J. Tückmantel, CERN/EF/RF 84-2.
- [18] E. Haebel, P. Marchand and J. Tückmantel, CERN/EF/RF 84-1.
- [19] T. Weiland, DESY Report 82-015 (1982) and M-82-24 (1982).
- [20] J. Tückmantel, CERN/EF/RF 83-5.
- [21] Ph. Bernard et al., CERN/EF/RF 83-6.
- [22] G. Guignard, CERN/LEP parameter Note 9 (version 13, phase 1, January 1984).
- [23] B. Zotter, Trans IEEE-NS 30, 2 (1983) 519.
- [24] W. Weingarten, this Workshop.
- [25] J. Schmid, this Workshop.
- [26] A. Schopper and W. Weingarten, CERN/EF/RF 83-7.
- [27] G. Sayag, T. Viet Nguyen, H. Bergeret and A. Septier, J. Phys. E10 (1977) 176.
- [28] P. Bernard et al., CERN/EF/RF 82-9 (1982).

TABLE 1

Some cavity parameters

	Iris opening diameter (mm)	R/Q (Ohm/m)	E_p/E_{acc}	H_p/E_{acc} (G/MV/m)	G (Ohm)	$K^{(a)}$
<u>500 MHz</u>						
1 cell	150	451	1.94	37.6	272	-
5 cell (PETRA)	150	443	2.05	37.7	272	0.9%
<u>350 MHz</u>						
1 cell	210	310	1.94	38	272	-
4 cell (LEP)	241	273	2.3	39.5	272	1.76%
<hr/> <p>(a) $K = \frac{f_{\pi} - f_0}{0.5 (f_{\pi} + f_0)}$</p>						

TABLE 2
Some experimental results

Type of cavity	Q_0 ($\times 10^9$) at low field		E_{\max} at E_{\max}		E_{\max} (MV/m)	Field limitation	λ (W/mxK) at 4.2 K	Remarks
	2.3 K	4.2 K	4.2 K	4.2 K				
<u>500 MHz</u>								
5 cell (PETRA cavity)	1.35	1	0.74	5	5.2	defect at welding (dust)	10.5	Vacuum accident
2 cell	2.7	1.8	1	6	6	defect at HOM coupling port	10.5	
1 cell (from PETRA cavity)	> 10	1.1	0.9	7.6	7.9		10.5	
1 cell H1	-	1.2	0.7	13 ± 0.9	-	e^- loading	28	Anodized
1 cell H2	5.7	1.6	0.6	> 8	> 8	e^- loading	28	Non-anodized
1 cell Nb Cu	7	1.8	0.3	8.6	-	Q degradation	> 300	No fast quench
1 cell TIG welded	5.4	1.3	1	4.2	4.2	defect at welding	10.5	
<u>350 MHz</u>								
No.1	18	4	3	5.4	6.4	electron loading	10.5	Defect at welding
No.2	8.2	4.1	3	5.4	5.4	electron loading	10.5	Not anodized
	6.3	3.2	2.4	5.6	5.6	electron loading	10.5	Anodized
<u>3 GHz (1.8 K)</u>								
1 cell EBW welded	5	-	2.1	-	9.9	Q degradation	28	
TIG welded	4.5	-	0.63	-	8	"	28	
5 cell TIG welded	7.5	-	-	-	4	defect at welding	28	

FIGURE CAPTIONS

- Fig. 1 Maximum field level E_{acc} achieved at the first cool down for single-cell 500 MHz cavities. Cavities have been submitted only to CP but a guided repair has been sometimes applied before the last CP.
- Fig. 2 Layout of multicell cavities:
- (a) Geometry of 500 MHz 5-cell cavity used for the PETRA test. Each cell is equipped with one HOM coupler. MC: main coupler port; E1, E2, E5: coupling ports for HOM electric couplers; H2, H3: coupling ports for HOM magnetic couplers; P1-P5: r.f. probes.
 - (b) Improved geometry of 350 MHz 4-cell cavity for LEP. MC: main coupler; EH1, EH2: HOM couplers; all couplers are located at the beam tubes.
- Fig. 3 New installation for chemical polishing and rinsing of multicell cavities. Acids are pumped and emptied from below, rinsing is performed by a sprinkler tube located inside the cavity.
- Fig. 4 The 500 MHz, 5-cell cavity (PETRA cavity) equipped with a T mapping system and a hydraulic tuner. The tuner is actioned by a membrane with GHe (and LHe) between the double plate at bottom and changes the total length of the cavity. Pumping is done from below.
- Fig. 5 Q_0 as a function of accelerating field for a 500 MHz cavity (H2) at 4.2 K before and after exposure to dust-free laboratory air. 1 cm³ of air corresponds to ~ 10 monolayers of adsorbed gas.
- Fig. 6 500 MHz cavity with improved λ (H1). Quality factor as a function of accelerating field at 4.2 K with anodization (100 V). The final values have been obtained after some r.f. processing and He-ion sputtering. The field is limited by electron induced quenches.

FIGURE CAPTIONS (Cont'd)

- Fig. 7** 500 MHz cavity with improved λ (H1): Temperature map taken at 12.6 MV/m. RF losses are dominated by frozen-in magnetic flux from the external magnetic field (130 mG). The weldings (indicated by arrows) cannot be distinguished from the surrounding regions except for 2 small defects. The quench is produced at the bottom iris (resistor R37).
- Fig. 8** Surface temperature near defect and flux cones (2% steps) for a defect with a radius of 0.2 mm and with a surface resistance $R_s = 1.2 \times 10^{-2}$ Ohm; bath temperature $T_b = 4.2$ K:
- (a) For a niobium wall with $\lambda = 10.5$ W/K x m. Under these conditions a quench would be produced at ~ 200 G ($E_{acc} = 5.28$ MV/m, $P_{diss} = 157$ W).
 - (b) For a niobium wall with $\lambda = 28$ W/K x m; a quench would be produced at ~ 300 G.
 - (c) For a copper wall with $\lambda = 485$ W/K/m; a quench would be produced at ~ 715 G. In this case tube cooling with a tube distance of many centimetres can be envisaged.
- Fig. 9** Photo of the 350 MHz cavity fabricated from 3 mm sheet niobium with its temperature mapping system. The small 3 GHz cavity is used for studying surface properties.
- Fig. 10** 350 MHz cavity: quality factor as a function of E_{acc} for different bath temperatures. The field is limited by an electron induced quench.

FIGURE CAPTIONS (Cont'd)

Fig.11 350 MHz cavity No. 2:

- (a) Temperature map taken at $E_{acc} = 4.8$ MV/m. A big defect can be seen which has been removed later on by a local electropolishing. A small defect is located at the welding.
- (b) as (a) with enlarged temperature scale showing r.f. losses due to the external magnetic field $H_{ext} = 130$ mG.
- (c) Thermography obtained by image processing from (a) for localising precisely regions with increased r.f. losses.
- (d) RF losses of all resistors summed up over the azimuthal angle ϕ . The loss distribution has a maximum at the equator ($s = 0$) and is dominated by frozen-in flux from H_{ext} .

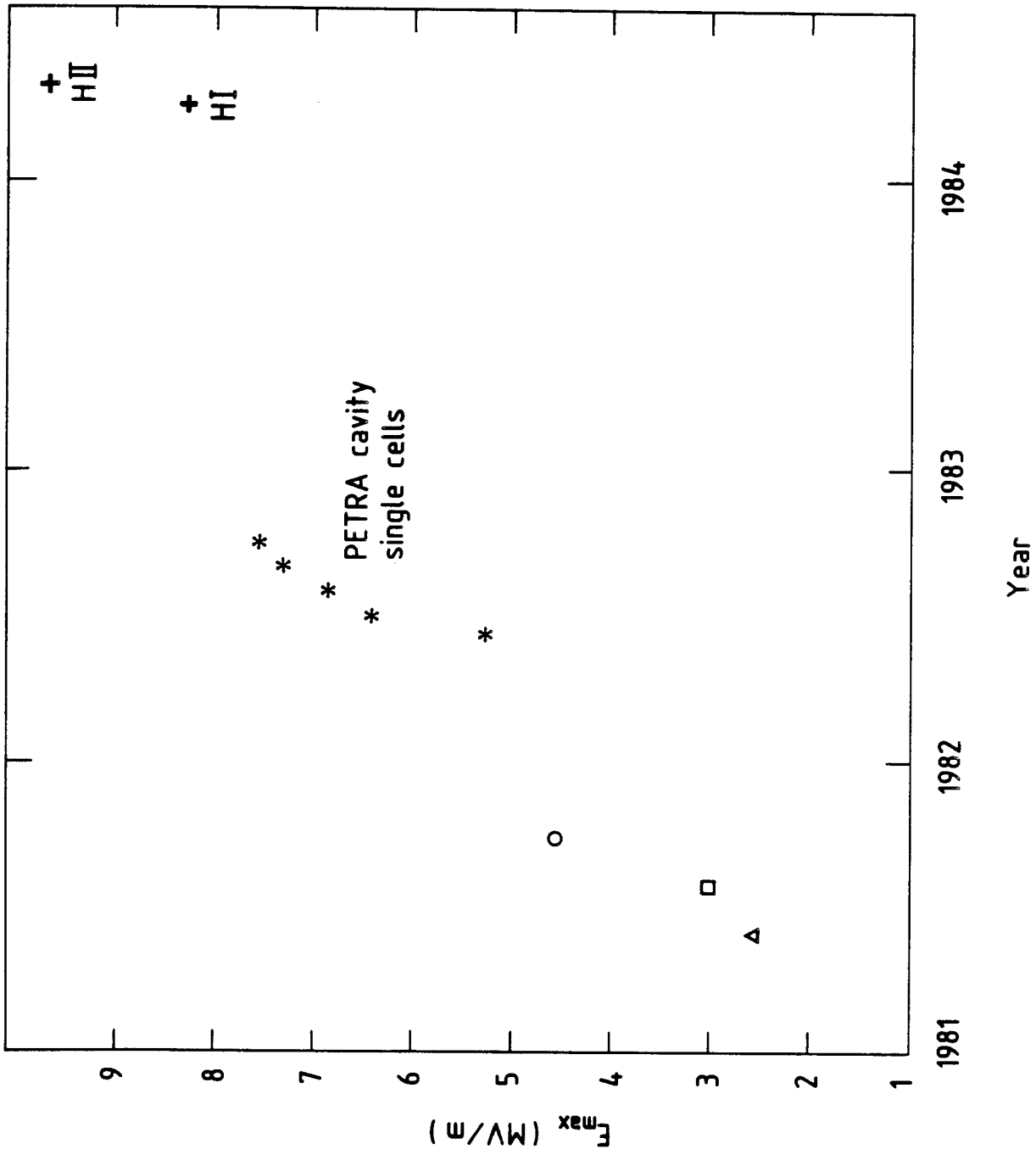


Fig. 1

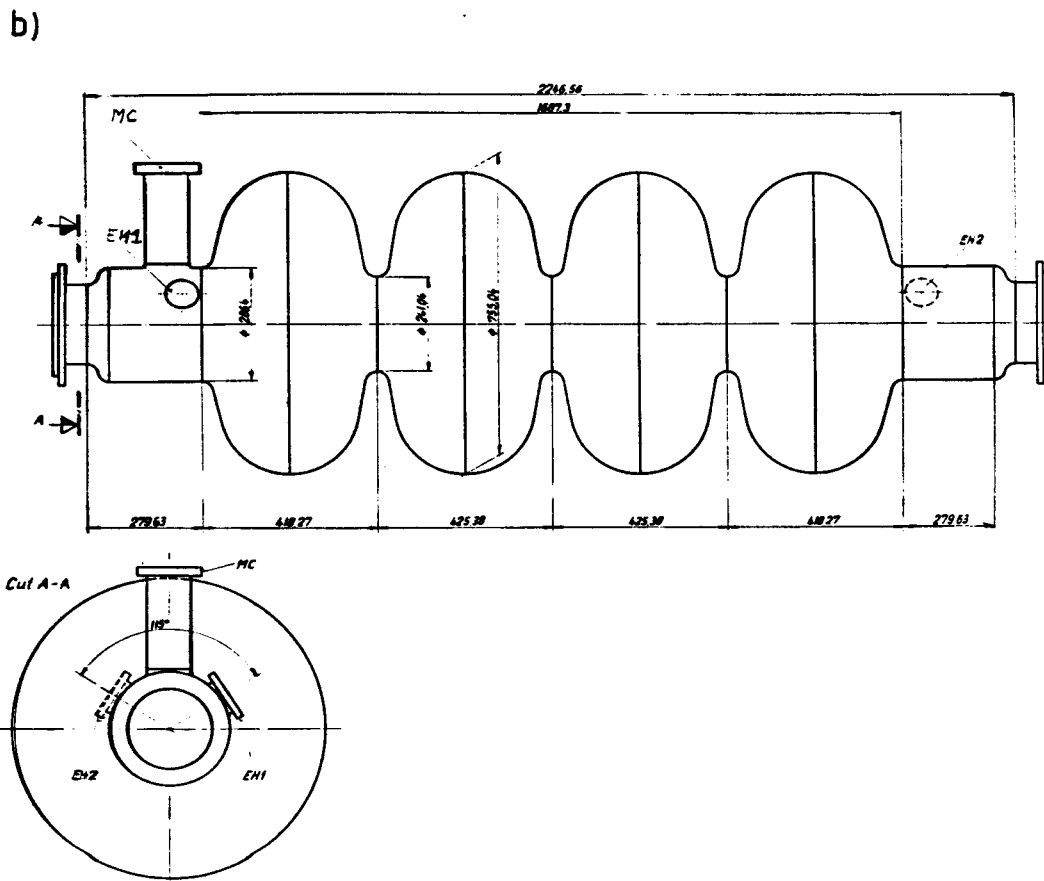
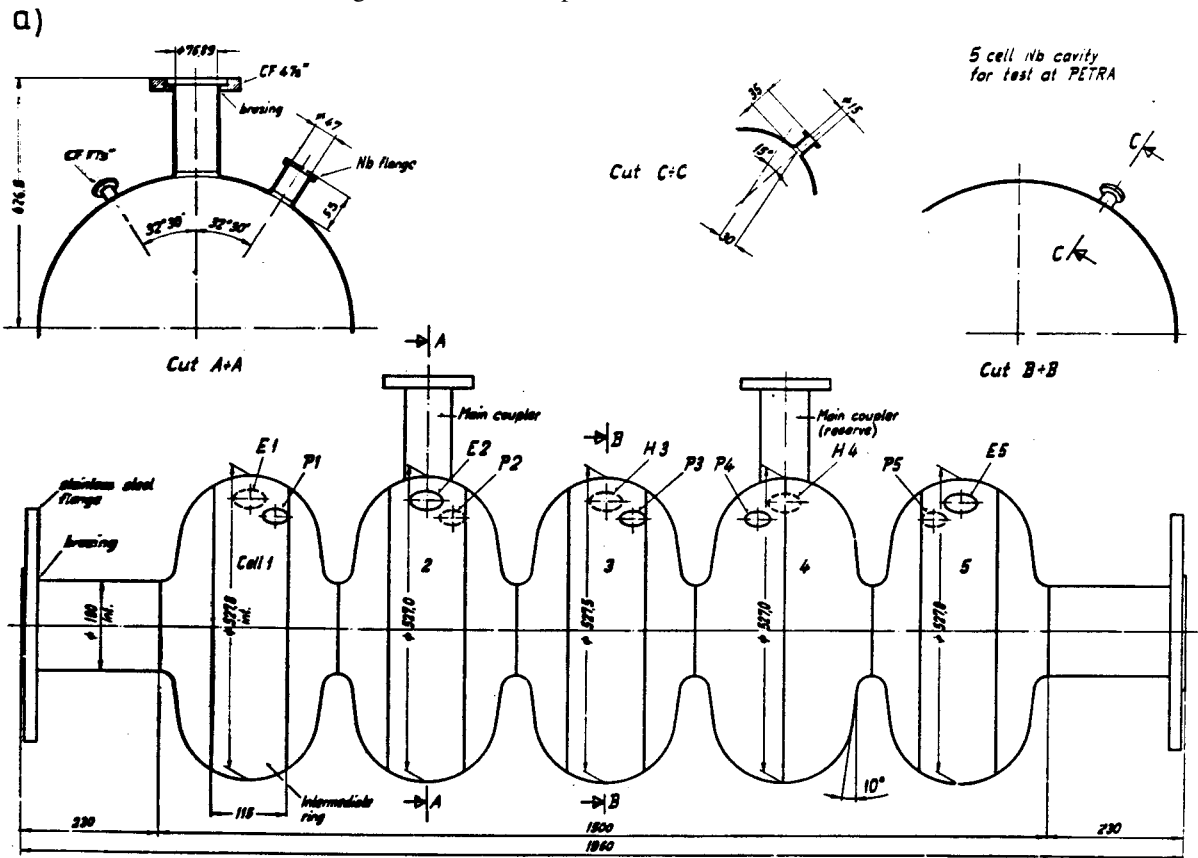


Fig. 2

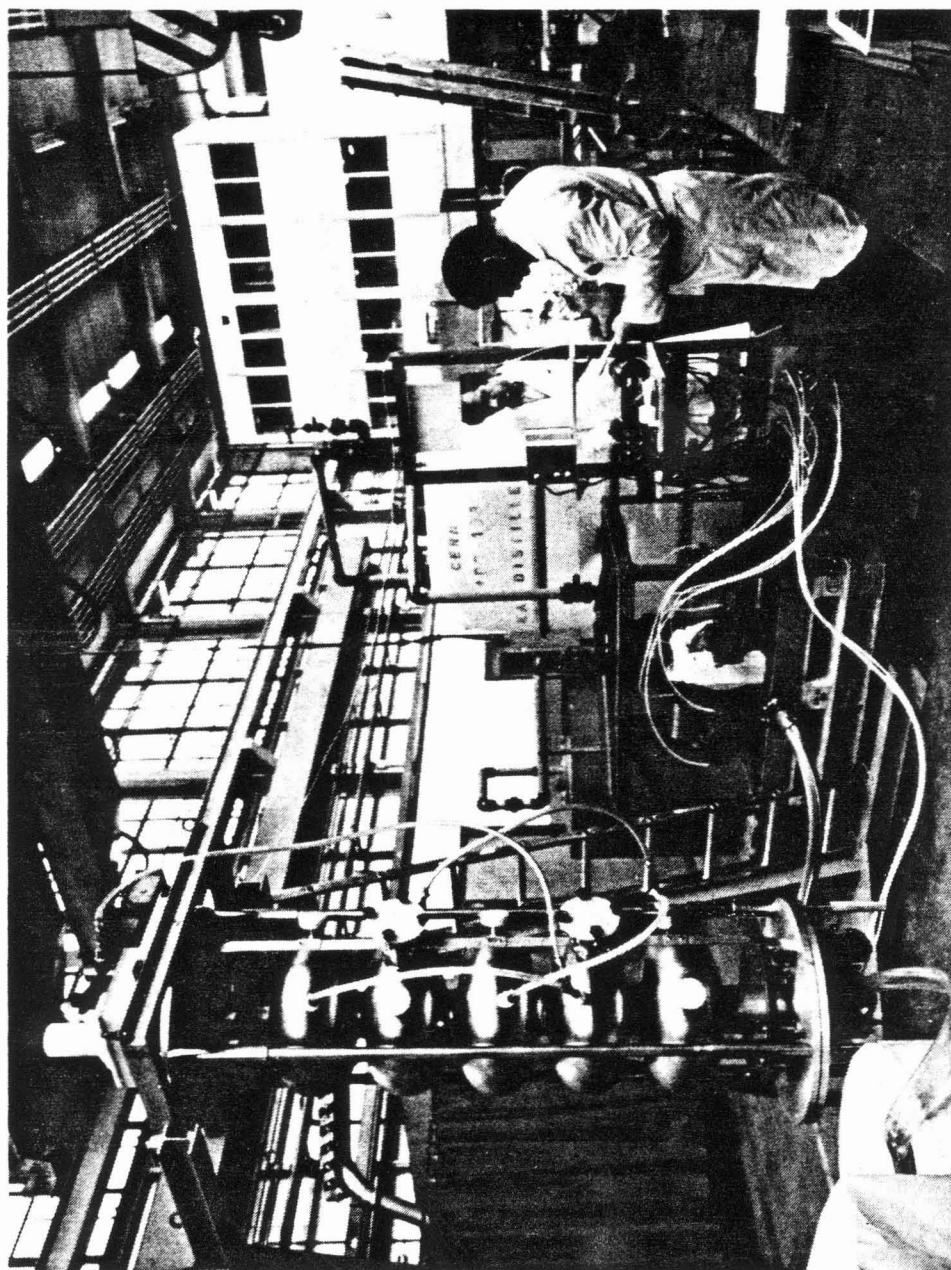


Fig. 3

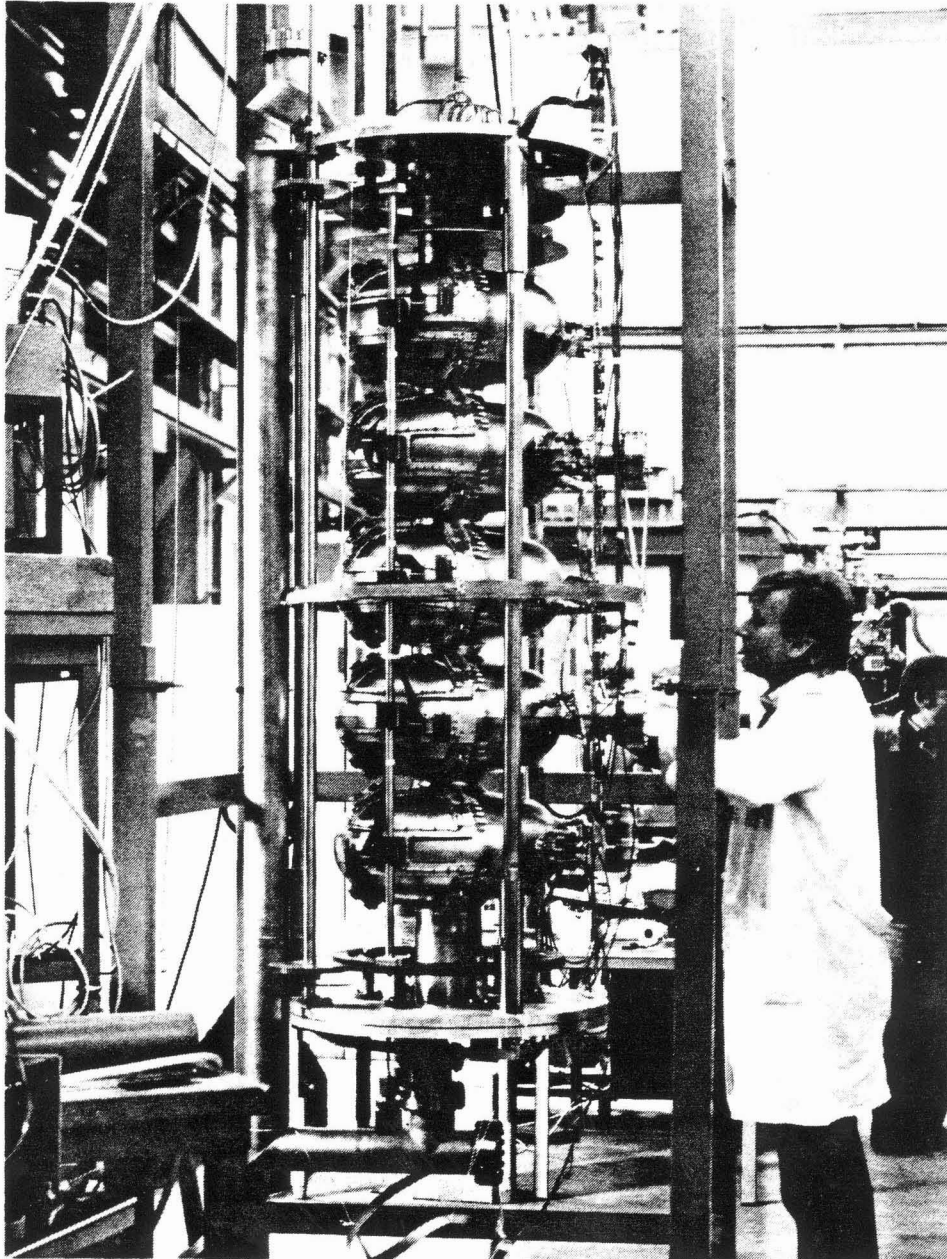


Fig. 4

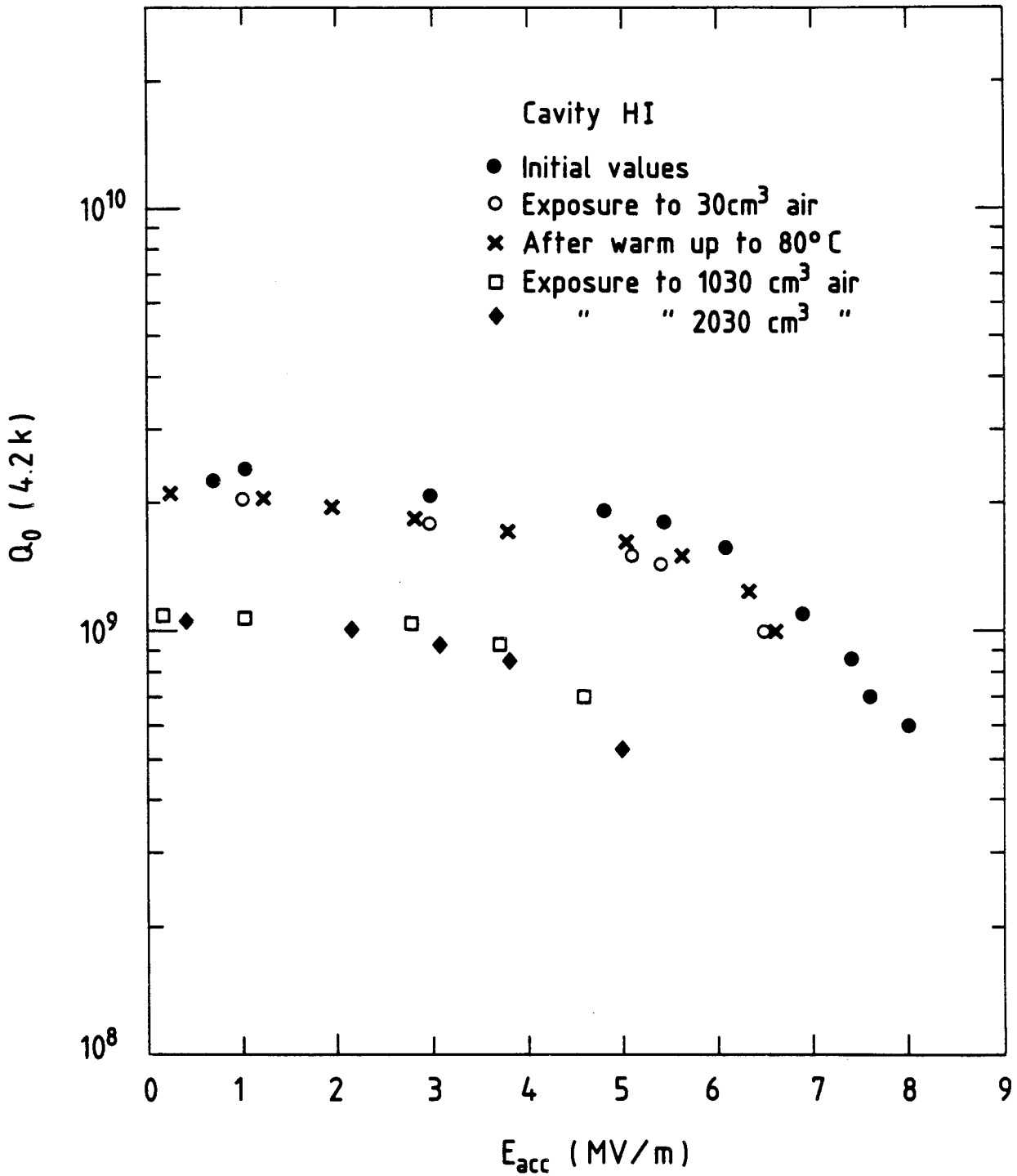


Fig. 5

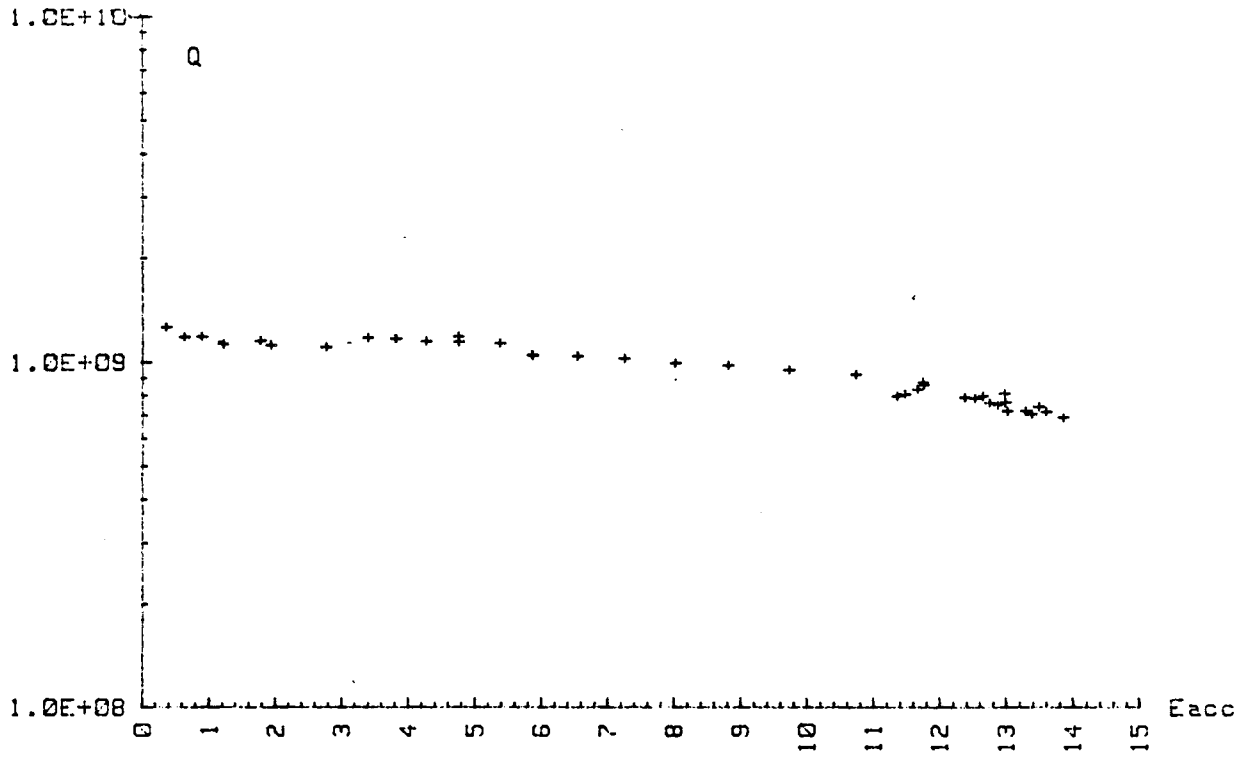


Fig. 6

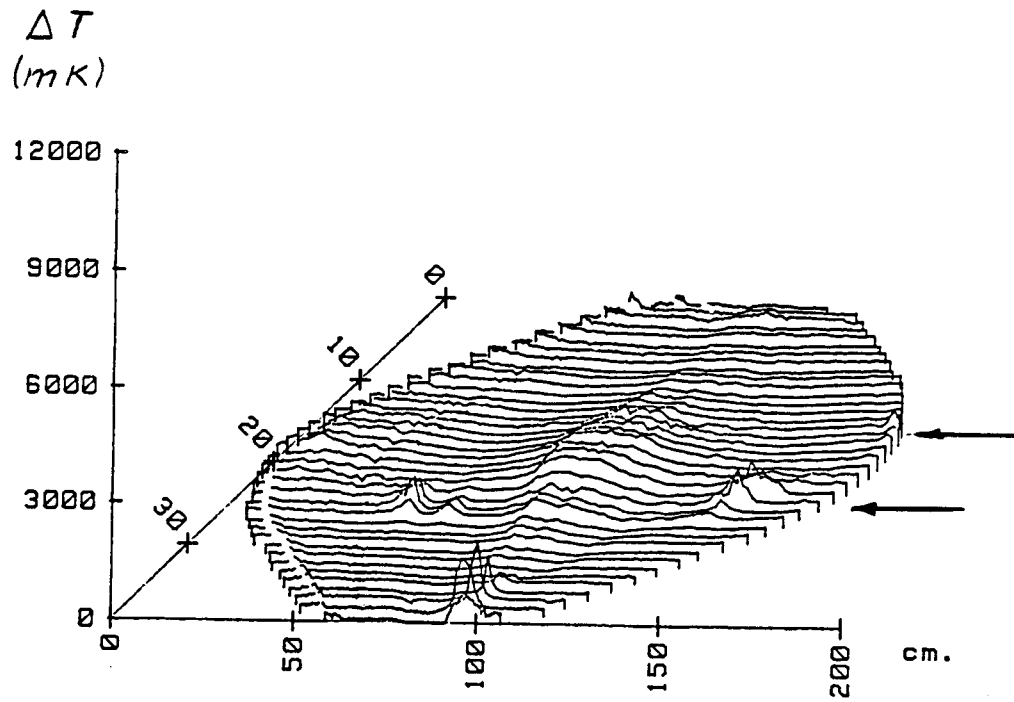
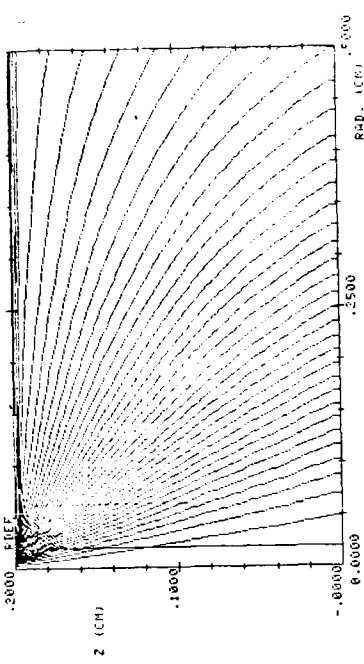
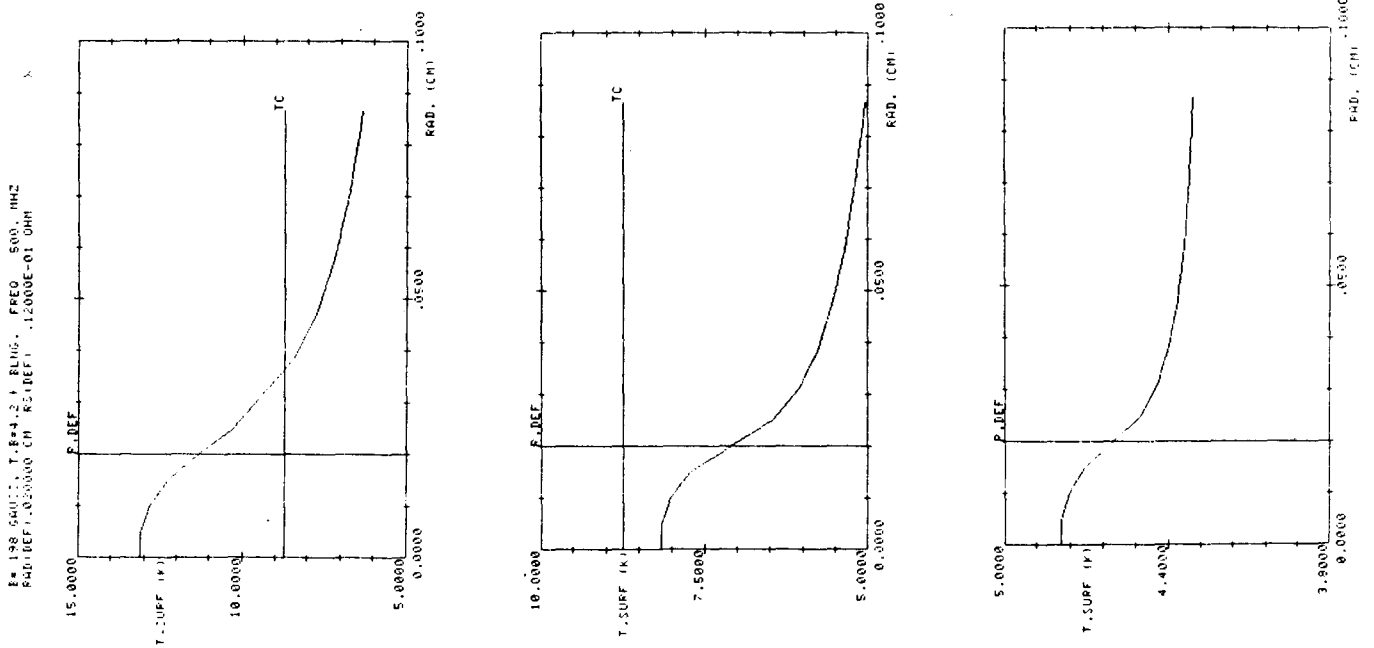
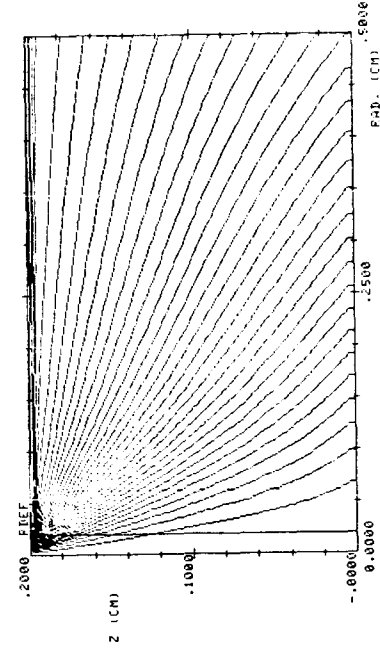


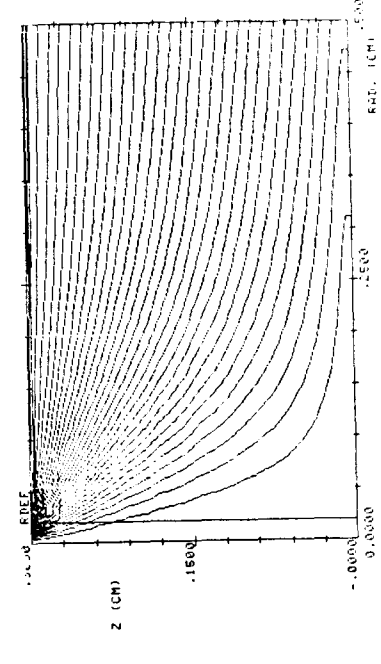
Fig. 7



a)



b)



c)

Fig. 8

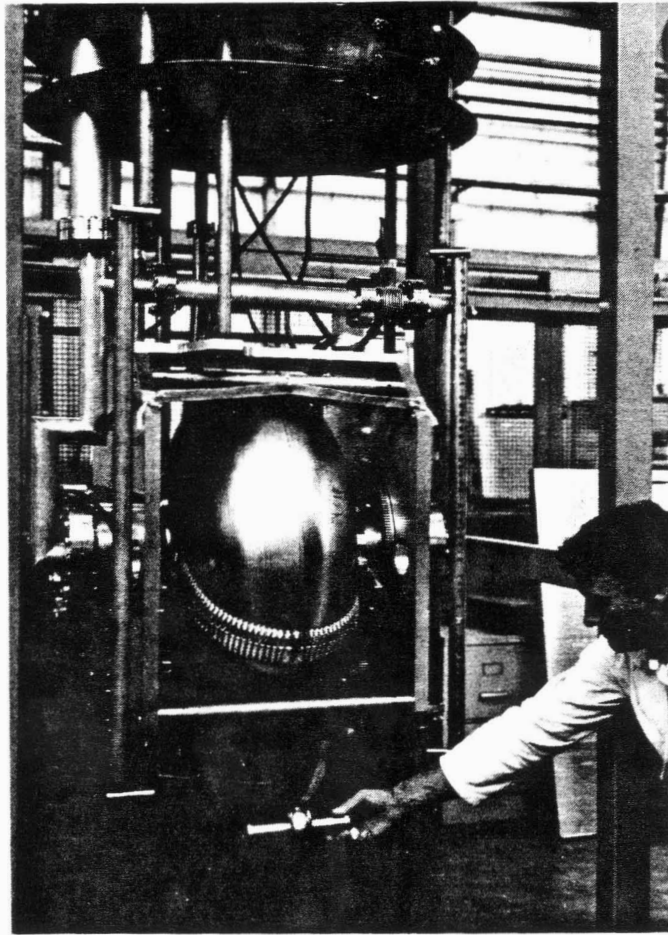


Fig. 9

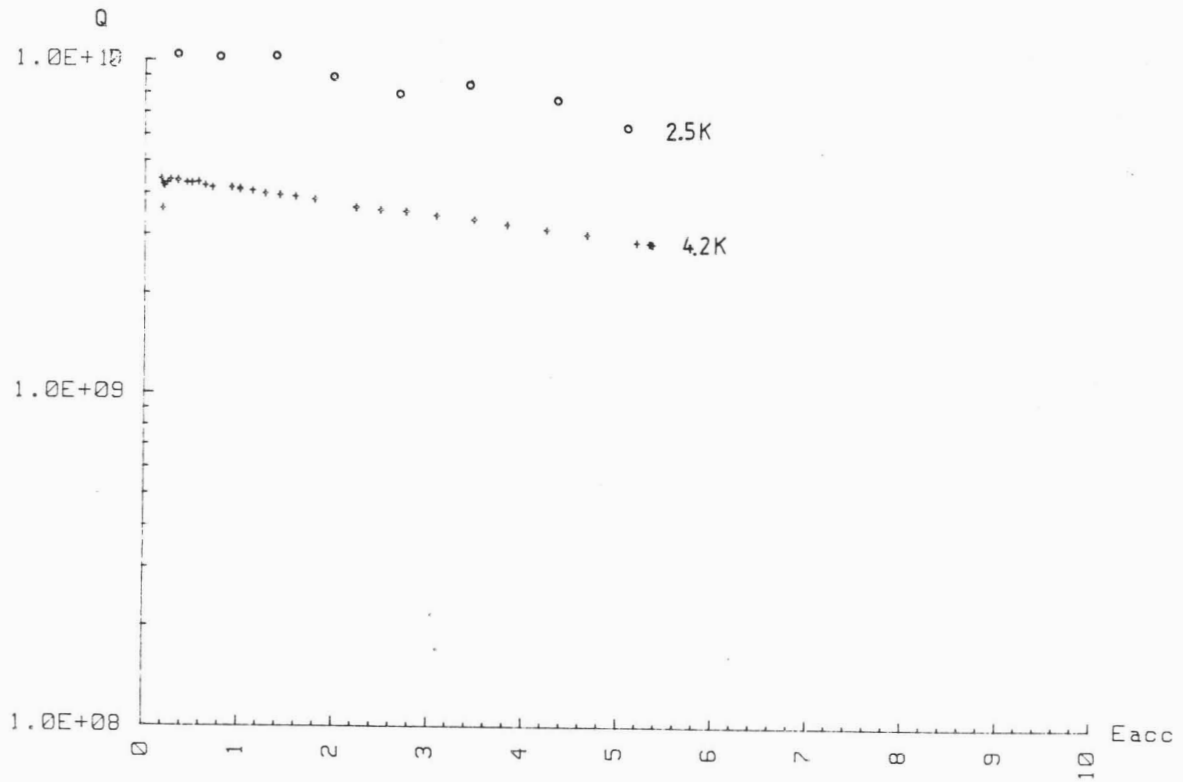


Fig. 10

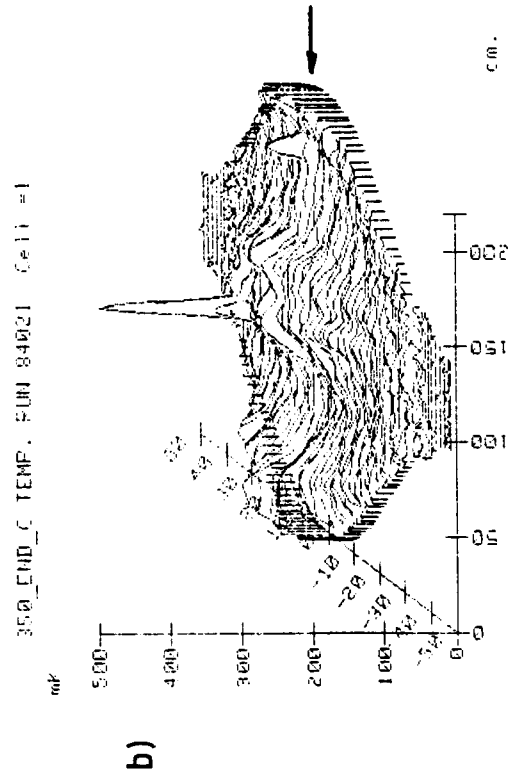
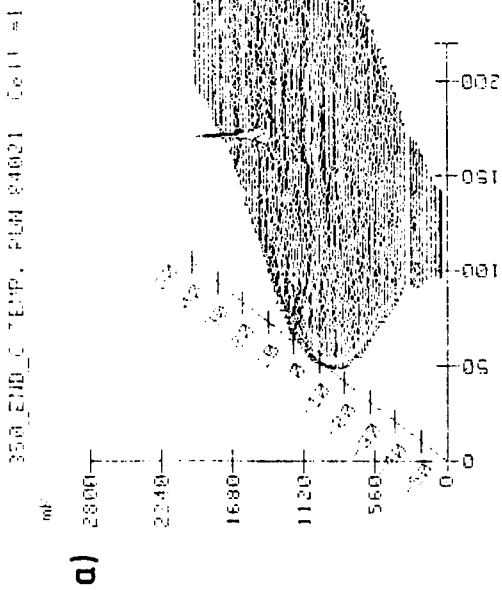
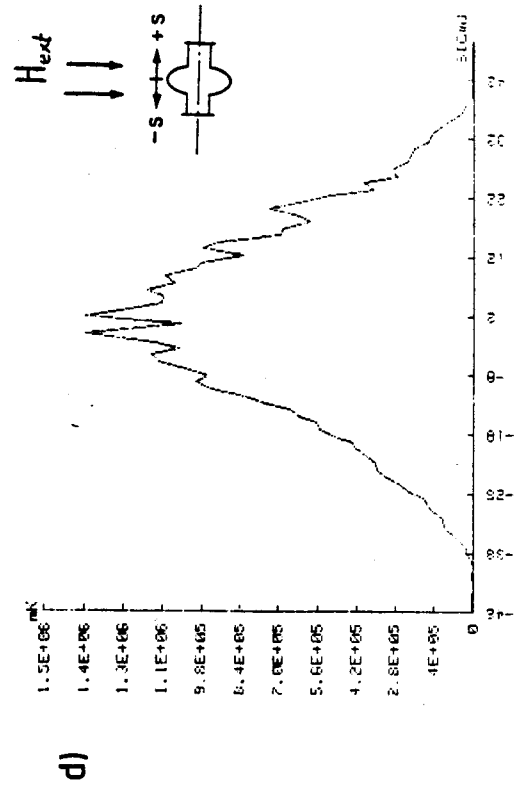
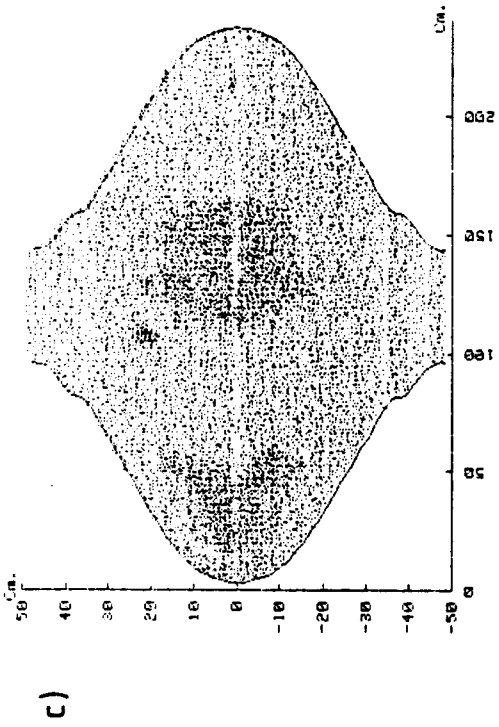


Fig.11